Final Report

Earthquake Commission Biennial contestable grants programme

Eruption history of Rangitoto volcano Project 3704187 (14/676)

Principal Investigator: A/P Phil Shane
Associate investigators: Shane Cronin, Jan Lindsay, Ian Smith

School of Environment, University of Auckland, Private Bag 92019, Auckland 1142

November, 2015

TECHNICAL ABSTRACT

Drilling through the edifice of Rangitoto, the youngest and largest volcano in the 'monogenetic' basalt Auckland Volcanic Field (AVF), reveals the multi-stage eruptive and magmatic history of a small shield volcano. *This is a major departure from our previous knowledge of the volcano.* Activity commenced up to 6000 cal years BP, involving minor effusive and pyroclastic volcanism. A voluminous shield building phase occurred 650-550 cal years BP, erupting isotopically-uniform sub-alkalic basalts (Mg# 60-64). Four batches of magma distinguished by trace element chemistry were erupted sequentially, but lack genetic connection via fractional crystallization or assimilation. Two of the magma batches display linear trends of decreasing incompatible trace element abundance and increasing ratio of moderately incompatible to highly incompatible elements with decreasing age. This is consistent with cycles of progressive partial melting at the source. The final phase of activity (~550-500 cal years BP) was explosive and less voluminous, producing scoria cones at the summit. This phase involved more diversity in magma compositions including more mafic sub-alkalic basalt, and alkali basalt, pointing to sourcing of magmas simultaneously from different depths in the mantle. Rangitoto's history and the lack of evidence for shallow magma residence demonstrate that deep lithospheric magma conduits can remain thermally and mechanically viable and/or be reactivated for volcanoes of low magma supply rate. Rangitoto volcano contributes to a growing body of evidence that major periods of volcanism in 'monogenetic' basalt fields occur at individual volcanoes that have experienced multiple eruption episodes, and erupt magmas that are compositionally diverse. Changes in magma composition accompany changes in eruption style, but a lack of an obvious shared pattern in magmatic evolution at various volcanoes points to the localized mantle heterogeneity and conduit systems. Hazard scenarios for regions traditionally classified as 'monogenetic' need to encompass the possibility of prolonged episodes of activity and reawakening of volcanoes, a significant implication where infrastructure is built on such regions.

LAYPERSONS ABSTRACT

Investigation of a 150-m-deep core drilled into Rangitoto volcano, Auckland, reveals a volcanic history extending farther back in time than previously known. The oldest lava flow has been dated by radiocarbon ages on wood and shell from enclosing estuarine sediments at about 6000 years old. Most of Rangitoto is made of a pile of lava flows constructed between 650 and 550 years ago. Traditionally it was thought that Rangitoto volcano had formed in one or two brief episodes about 550 years ago. However, the rocks in the drill core suggests this was a late phase of activity that post-dates most of the volcano's construction. The prolonged and perhaps episodic activity is consistent with the studies of microscopic ash from Rangitoto preserved in sediments at Lake Pupuke. The composition of magma erupted from Rangitoto has changed with time due to processes of melting in the mantle. However, there no evidence of interaction between the rising magmas and Earth's crust. This implies the magmas ascend fast and there would be limited warning times in any future eruptions. However, this new study means hazard scenarios for regions traditionally classified as 'monogenetic' need to encompass the possibility of prolonged episodes of activity and reawakening of volcanoes, a significant implication where infrastructure is built on such regions.

INTRODUCTION

This study focuses on Rangitoto volcano of the Auckland Volcanic Field (AVF) in New Zealand (Fig. 1). It is composite basalt edifice comprising a radial lava field and scoria cones that has erupted multiple batches of magma (Needham et al., 2011), and thus, does not

fit the traditional monogenetic classification. As a large urban region (Auckland City) is built on it, the AVF has been the focus of numerous petrological (e.g., Smith et al., 2008; McGee et al., 2011; 2012; 2013), and hazard/risk studies (e.g., Houghton et al., 2006; Bebbington and Cronin 2011). This prompted a drilling project to recover a complete stratigraphic sequence of an AVF volcano. Rangitoto volcano was selected as is the youngest in the AVF, last erupting at ~550-500 cal yrs BP (Needham et al., 2011). Furthermore, the volcano is anomalous because of its size relative to the rest of the AVF, comprising ~0.7 km^3 of the ~1.7 km^3 of magma erupted in the field (Kereszturi et al., 2013). Yet little is known about its eruption history and how it was constructed. The main edifice of the volcano has been variously classified as a scutulum-type lava shield (Walker, 1993) or an amalgamation scoria cones (Needham et al., 2011). The duration of volcanism has been inferred as either brief (~50 years, Needham et al., 2011) or long (>1000 years, Shane et al., 2013) based on various chronological constraints. Understanding which of these two growth histories applies to Rangitoto is essential to defining future eruption hazard models for the AVF that either treat it as extinct, or potentially a site of a future repeat eruption. This has implications for other basaltic fields that contain complex 'monogenetic' volcanoes and/or small shields (e.g., Boyce, 2013).

BACKGROUND

The AVF is situated in a continental intra-plate setting with a crustal thickness of ~30 km, and overlying a zone of lower S-wave velocities at a depth of 80 km (Horspool et al., 2006). The field comprises ~50 basaltic cinder cones, maars, and associated lava fields, with an estimated total volume of magma erupted of ~1.7 km^3 (Kereszturi et al. 2013). The known vents are scattered over a 360 km^2 area (Fig. 1A). Activity commenced at ~250 ka and continued intermittently to ~0.5 ka.

Rangitoto Island (volcano) is a symmetrical, ~6 km wide, structure rising ~260 m above sea level (Fig. 1B), with a dense-rock volume of about 0.7 km^3 (Kereszturi et al. 2013). A broad negative bouguer gravity anomaly, albeit based on limited data, led Milligan (1977) and later Needham et al. (2011) to infer that much of the volcano is built from lower density pyroclastic material overlain by a thin (<40 m) lava carapace. However, this contrasts with Walker's (1993) interpretation of a lava shield. The summit region comprises a scoria cone (Central Cone) flanked to the north and south by remnant scoria mounds and ridges from older cones (North and South Cones). Much of the edifice comprises gently dipping (~12° near summit to ~4° near the coastal flanks) pahoehoe and aa lava fields. The Central and South Cones erupted sub-alkalic basalts of narrow compositional range (~48–50 wt. % SiO_2), while the North Cone erupted lower-SiO_2, alkalic basalt (~45–47 wt. %) (Needham et al., 2011). The lava field also comprises sub-alkalic basalt. Geochemical and isotopic parameters indicate the two compositions represent separate magma batches derived from various depths in the mantle (McGee et al., 2011, 2013). However, the eruption sequence is poorly exposed due to the lack of erosional dissection.

Tephra layers occur as scattered exposures and in sediment cores surrounding the volcano. Early sediment coring revealed two macroscopic basaltic tephra layers (Needham et al., 2011). The lower layer was considered to have an alkalic basalt composition based on bulk-ash analyses, while a single bulk-ash analysis of the upper tephra was reputed to be sub-alkalic basalt. Thus, reflecting the bimodality of magma compositions erupted from the volcano, and providing a basis for the stratigraphic order of the magma eruption. Volcano construction was inferred by Needham et al. (2011) as follows: (1) formation of an alkalic basalt scoria cone (North Cone); (2) formation of a larger scoria cone from a nearby vent erupting sub-alkalic basalt (Central and South Cones); and (3) an effusive phase of lava producing a thin veneer over the edifice (Fig. 1C). As the two macroscopic tephra layers in

sediment cores were dated at about 550 and 500 cal years BP, the eruptions of the two magma batches were considered to be separated by about 50 years. However, as discussed by Shane et al., (2013), pyroclastic fragmentation and hydraulic sorting of glass and crystal components in tephra make the classification of bulk ash compositions as alkalic or sub-alkalic problematic. In particular, some samples contain abundant olivine crystals, and others contain accidental ejecta such as shell fragments and detrital sediments.

Compounding the uncertainty associated with tephra stratigraphy has been the assumption that the tephra layers represent the condensed eruptive history of the entire volcano (summarized by Nichol, 1992; Lindsay et al., 2011). As noted by Shane et al. (2013) some of these ages are stratigraphically inverted, making their interpretation equivocal. Studies of Rangitoto-sourced microscopic tephra in lake sediments indicate a longer multi-phase eruptive record, perhaps extending from about 1500 to 500 years ago (Shane et al., 2013).

METHODS

The drill site is located at metric grid North 5927446, East 1765100 (map NZTopo50-BA32, Edition 1.02), about 120 m above sea level on the western flank of the volcano (Fig. 1B). Drilling was performed using a skid-mounted ADL Series HD900 Drilling Rig. The 0 to 114.90 m depth interval was drilled using PQ triple tube (122.6 mm diameter), while HQ triple tube (96 mm diameter) was used for the 114.90 to 148.10 m depth interval, with the PQ rods remaining in place to support the hole. Recovered core widths were 85 mm (HQ) and 63.5 mm (PQ). Recovery is estimated at >95%.

Sixty-eight rock samples were collected, many in duplicate, representing 36 dense lava flow units and two scoria clasts, from various depths in the core (Fig. 2). Rock samples for geochemical analyses were crushed in a tungsten carbide ring grinder. The whole rock powders were fused into disks following the Norrish fusion method (Harvey et al., 1973) with a dilution factor of 2:6 (ignited sample to 12:22 lithium tetraborate: lithium metaborate flux). The disks were analyzed in triplicate using a Panalytical Axios 1 kW wavelength dispersive XRF spectrometer at the University of Auckland, with an Rh tube to obtain major elements. Twenty-eight international standards analyzed in triplicate were used for calibration. USGS glass standard BCR-2G was analyzed to provide an independent assessment of accuracy and precision (see supplementary data). The results for BCR- 2G are consistent with the reference values within <1% for elements used in this study, and replicate analyses indicate an analytical precision (2σ) of <1% (mostly ~0.7 %).

Whole rock trace element analyses were determined by laser ablation inductively-coupled mass spectrometry (LA-ICPMS) at the Australian National University, using an Excimer LPX120 laser and Agilent 7500 series mass spectrometer. Analyses were performed on XRF discs, following the procedure of Eggins et al. (1998). The NIST 612 glass, analysed after every 15 unknowns, was used as primary calibration standard while BCR-2G was analysed to provide an independent assessment of accuracy and precision (see supplementary data). The results for BCR- 2G are consistent with the reference values within 10 % for elements used in this study (mostly ~5%), and replicate analyses indicate an analytical precision (2σ) of about 5 % for most elements, except for Zr , Cr, Ni and Pb (>10%).

Radiogenic isotope analysis on selected whole rock samples were performed at the University of Melbourne, using procedures similar to those described in Maas et al. (2005) and Van Otterloo et al. (2014). Handpicked rock chips were leached with 6M HCl (100C, 1 hr), rinsed with distilled water, and dissolved in 2 ml mixed HF-HNO_3 (3:1). After evaporation of the HF, the residue was refluxed twice with conc. HNO_3 before dissolution in 6 ml of 5M HNO_3. Isotopic analyses were carried out on a Nu Instruments Plasma multi-collector inductively coupled plasma mass spectrometer (MC-ICP-MS) coupled to a CETAC

Aridus desolvator. Instrumental mass fractionation in Sr and Nd runs was corrected by internal normalization to $^{88}Sr/^{86}Sr=8.37521$ and $^{146}Nd/^{144}Nd=0.7219$ using the exponential law; final $^{87}Sr/^{86}Sr$ and $^{143}Nd/^{144}Nd$ are reported relative to SRM987 = 0.710230 and La Jolla Nd = 0.511860, respectively. Typical internal (2se) precision is ±0.000020 for $^{87}Sr/^{86}Sr$ and ±0.000010 for $^{143}Nd/^{144}Nd$, while external precision (reproducibility, 2sd) is ±0.000040 and ±0.000020, respectively. Instrumental mass bias in Pb isotope analyses was corrected using the thallium-doping technique of Woodhead (2002) which provides external precisions (2sd) of ±0.05% for $^{206}Pb/^{204}Pb$ and $^{207}Pb/^{204}Pb$, and ±0.08% (2σ) for $^{208}Pb/^{204}Pb$. Results for standards (e.g. BCR-2 0.704997±42, 0.512641±24, 18.758±9, 15.619±10, 38.726±35, all errors ±2sd, based on 40 or more analyses over several years) are consistent with TIMS and MC-ICP-MS reference values.
Organic material was collected from marine sediments for radiocarbon dating. The material was collected from the middle of the core sections at least 30 cm from the ends of the core runs to minimize the possibility of contamination due to the drilling process. AMS radiocarbon dating was undertaken at the Rafter Radiocarbon Laboratory, New Zealand. Shell samples were cleaned and acid etched, followed by generation of CO_2 and conversion to graphite for AMS analysis. The wood and seed samples were cleaned and underwent acid/alkali/acid pretreatment prior to analysis. The AMS ^{14}C ages were calibrated with OxCal 4.2 using the SHCal13 calibration (Hogg et al., 2013) for the wood and seed samples, and Marine13 (Reimer et al., 2013) for the shell.

RESULTS

Lithology of the core sequence

Recovery of Miocene sediments at the base of sequence demonstrates the entire edifice beneath the drill site was penetrated. The upper 128 m of the sequence comprises massive basaltic lava flow units separated by basaltic breccia (Fig. 2). The breccia consists of highly fractured and angular clasts (<1 cm to 10 cm in size) with very little matrix (<10 %). Some fracturing is in situ. Contacts between the breccia and massive lava are generally gradational over depths of 5-10 cm, and some contacts display welding of clasts on the flow unit. By comparison to surface outcrops, the breccia are considered to represent autobrecciated zones formed at the top and base of lava flow units during flow emplacement. At least 53 dense lava units are thus recognized; these have thicknesses in the range <0.5 to 7 m (mostly about 1-2 m). They are light to dark grey and generally lack alteration. A few display red oxidation coloration, but there is no systematic pattern in alteration or coloration with depth in the sequence. The lavas range from dense and non-vesicular to highly vesicular (up to 30% vesicles and vugs). Some individual flow units display this range in vesicularity. Flow banding is evident in a few units and some dense units display sub-vertical joints. Breccia units (mostly < 1 m thick, max 5 m) mostly display red-to yellow oxidation colorations. Clasts in the breccia are notably more vesicular than the adjacent flow units.

The lava sequence of the upper 128 m of core lacks unambiguous evidence of depositional hiatus such as paleosols, and pyroclastic units are not observed. One exception is clay-filled fractures developed into the upper 1 m of a lava flow unit about 95 m depth, which may reflect a period of weathering.

The base of the lava flow sequence at 128.1 m is marked by a sharp contact between lava and fragmented fossil marine shells in ash overlying 20 cm of fossiliferous olive-grey mud (Fig. 2, 3). A basaltic volcaniclastic (pyroclastic?) sequence between 128.3 and ~135 m, comprises unconsolidated, poorly-sorted black ash to coarse lapilli. The lapilli are mostly sub-rounded to sub-angular blocky clasts displaying a range of vesicularity. Shell fragments and sedimentary grains occur in the ash-grade fraction. The unconsolidated character of the deposit and disruption from drilling prevents any assessment of stratification. Thin mud layers

(10 cm thick at 132.2 m, and 40 cm thick at 133.0 -133.4 m), seemingly divide the volcaniclastic unit. The interval 135.4-140.3 m depth is a continuous massive and fossiliferous, olive-grey sandy mud sequence. This unit contains a thin (~60 cm) massive lava flow unit (136.7-137.2 m depth). The sequence beneath 140.3 m is highly weathered Miocene sandstone and mudstone.

Radiocarbon ages

Thirteen samples were selected from the interval containing organic material (128-139 m depth) for dating via the AMS ^{14}C technique (Fig. 3; Table 1). The organic materials variously comprise single mollusca fragments, complete gastropod shells, a seed case and a wood fragment. Duplicate age determinations from different specimens at the same stratigraphic position produced concordant ages, including shell fragments and whole gastropods, and a shell fragment and wood. A concordant sequence of ages from ~7400 to 5900 cal yrs BP was obtained for estuarine muds at ~139.5-136.5 m depth. However, ages from mud layers associated with volcaniclastic deposits at ~135.5-128 m depth are stratigraphically inverted.

Geochemistry chemistry of basalts

Basalts from the core sequence display a narrow compositional range in major elements (SiO_2 ~48-49 wt %, normalized water-free; Mg# 0.60-0.64), and classify as sub-alkalic (Fig. 4A). Due to the narrow range of major elements, compositional trends are poorly defined on variation diagrams. In general, Al_2O_3, TiO_2, CaO, Zr, Hf, and Sr decrease, and Ni and Cr increase, with increasing Mg# (examples shown in Fig. 5). Many other elements, including incompatible elements such Nb, Th, Pb and rare earth elements (REEs) show little systematic variation with Mg#. The relative enrichment in high field strength elements (HFSE) Th, U, Pb, Nb and Ta on a primitive mantle-normalized multi-element plot and lack of negative Nb and Ta anomalies (Fig. 4B), is characteristic of intra-plate basalts as described previously for Rangitoto rocks (Needham et al., 2011; McGee et al., 2011). All of the basalts display relative enrichment of LREE and depletion of HREE (chondrite-normalized).

Clustering of basalt compositions on variation diagrams of nearly all major and trace elements allow four coherent compositional groups in the core to be defined (Fig. 5). The compositional groups relate to stratigraphic order in the core: Group 1 (137-95 m depth), Group 2 (93-69 m depth), Group 3 (67-26 m depth) and Group 4 (26-0 m depth) (Fig. 6). Included in Group 1 are scoria from the volcaniclastic deposit (128-135 m depth) and the isolated lava flow unit at 137 m depth. Features distinguishing the Groups include: relative enrichment in Nb, Ta, Ba, U, Th, Rb, and REE in Group 1; and enrichment in Ti, Sr, Zr, and Hf and low Mg# (<0.62) in Group 4. Groups 2 and 3 are somewhat similar in composition, but the former is distinguished by lower Mg#, Ni and Cr (Fig. 5). There is considerable temporal variation within both Group 2 and 3, including prominent upward stratigraphic trends of decreasing incompatible element abundance, e.g., Nb (18.5-12.5 ppm), Sr (326-287 ppm), and most REEs (Fig. 6). Ratios of incompatible elements, such as Zr/Nb (6.2-9.0) and Nd/La (1.2-1.39) in Group 2, increase upward in the stratigraphic sequence of both groups (Fig. 6). In contrast, Groups 1 and 4 lack within-group temporal trends.

Basalts in the core sequence are compositionally similar to those in surface outcrops of the lava field and Central and South Cones, but are compositionally distinct from the lower SiO_2 and higher Mg# composition of North Cone (Fig. 4A, 7). In addition, the Central Cone displays a few higher Mg# compositions not represented in the sub-surface sequence.

The basalt sequence in the core is isotopically homogeneous with variation in Sr-Nd-Pb-isotopes barely exceeding analytical error (Table 2; Fig. 7): ^{87}Sr-^{86}Sr = 0.702969 to 0.703069; ^{143}Nd-^{144}Nd = 0.512939 to 0.512983; ^{206}Pb-^{204}Pb = 19.037-19.067; ^{207}Pb-^{204}Pb =

15.587-15.603; and ^{208}Pb-^{204}Pb = 38.729-38.779. These isotopic compositions are in the range previously reported for Rangitoto basalts, and are similar to basalts from other volcanoes in the AVF (Huang et al., 1997; McGee et al. 2011, 2013). As described by these workers, Sr-Nd isotope signatures plot near the Pacific MORB- HIMU field boundaries (Fig. 4C), and Pb-isotope ratios place the rocks on the more radiogenic end of the MORB field between Pacific MORB and HIMU, and close to New Zealand lithospheric compositions. A sample from North Cone analyzed here is somewhat distinct, displaying slightly more radiogenic isotopic ratios (Table 2; Fig. 4C).

DISCUSSION

Structure of the volcano

Some workers have inferred that the edifice of Rangitoto comprises an amalgamation of scoria cones, overlain by a thin veneer of late-stage lava flows (Mulligan 1977; Needham et al., 2011). However, drilling demonstrates that the edifice mostly comprises a lava shield (Fig. 1C), consistent with Walker's (1993) interpretation. The drill site is located ~ 120 m above sea level on a lava field that extends another 30-40 m in elevation before the topography is defined by scoria cones. Hence, although the depositional slope of the lava flows is unknown, the location of the drill site indicates that most of the edifice beneath the lava field was drilled. The sub-surface sequence comprises 128 m of lava flow units that overly about 8 m volcaniclastic deposits on pre-eruption strata (Fig. 2, 3).

The composition of the sub-surface basalts provides some insight to the completeness of the eruptive record because they mostly compositionally match basalts in surface outcrops. In particular, surface samples from the lava field and the Central Cone match compositional sub-surface Groups 2, 3 and 4, and scoria from the South Cone match Groups 2 and 3 (Fig. 7). A few high-Mg# Central Cone scoria samples do not have a compositional equivalent in the sub-surface sequence. The more alkalic, low-SiO_2 and high-Mg# compositions of the North Cone are also not represented in the sub-surface sequence. Sub-surface Group 1 lava compositions are not represented in the surface sample suite, presumably because of their early emplacement and subsequent burial in the lava pile. The spatial distribution of surface outcrops in the lava field and their composition indicates that the sub-surface lava sequence is widely distributed into various sectors of the volcano, and thus represents the incremental growth of the shield over several episodes of volcanism (Fig. 1B).

The scoria that lack compositional equivalents in the sub-surface sequence could point to emplacement post-shield. Notably, these scoria compositions are more mafic (high Mg#), despite the North Cone deposits being distinguished from Central Cone deposits by lower SiO_2 and higher alkali contents (Fig. 7). In contrast, scoria compositions from Central and South Cones with chemical affinity to sub-surface Groups 2-4 could imply contemporaneous scoria cone and lava field growth. The lack of stratigraphic control at the surface sampling locations (Needham et al., 2011), and the potential for syn- and post- eruptive recycling of ejecta in the vent region, prevents a chronological reconstruction of the magma emission at the scoria cones.

The thick lava pile encountered in the core and the lack of North Cone-like magma compositions in the sub-surface sequence do not support previous interpretations that the summit cones were constructed first. The proximity of the drill site to the summit scoria cones would have allowed the flanks of these cones to be encountered if they extended to sea level beneath the lava field as suggested by previous workers. In addition, tall scoria cones (up to 260 m above sea level) are unlikely because the topographic expression of the intact Central Cone with a crater diameter (W_{CR}) of ~190 m and cone basal width (W_{CO}) of ~500 m are typical of cinder cone dimensions ($W_{CR} = 0.40W_{CO}$, (Wood 1980)), and inconsistent with an

additional buried structure. Thus, the cones are most likely the youngest feature of the shield volcano.

The earliest volcanic deposit in the core sequence is a thin lava flow deposited in estuarine sediments (Fig. 3). This is overlain by basaltic volcaniclastic deposits. Phreatomagmatic activity may have been expected to be the first style of activity during an eruption in an estuary (~10-20 m deep based on modern bathymetry). However, the exact location of the initial vent is unknown, and pyroclastic deposits pre-dating the lava flow may be buried in other areas beneath the shield.

Chronology

Ages from the cored marine sediment sequence below 128 m-depth provide new insights to the chronology of Rangitoto volcano. Marine shell fragments, whole gastropods with delicate structure and a wood fragment provide a concordant sequence of ages from ~7400 to 5900 cal yrs BP for the estuarine muds at ~139.5-136.5 m depth (Fig. 3). These radiocarbon ages indicate that the oldest lava flow unit (at 137 m depth) was emplaced between ~6,800 to 5,900 cal yrs BP. This is considerably earlier than the previous "old" estimates of Rangitoto volcano (up to 1,500 cal yrs BP, Shane et al., 2013).

The ages collected from the mud layers intercalated with volcaniclastic (possibly pyroclastic) deposits at ~135.5-128 m depths are stratigraphically inverted, and generally increase in age up the core sequence (Fig. 3). Coring and fluidized extrusion of the non-consolidated pyroclastic material could have disrupted the sequence making this part of the sequence unreliable for development of an eruption chronology. However, the samples were collected from the middle of intact core sections, and away from disturbed ends of coring runs, so that such an issue is unlikely to be the cause of the apparent age inversion.

An alternative explanation is that the volcaniclastic deposits and associated mud layers represent mass-flow units, emplaced by slumping from a sub-marine pyroclastic structure. For example, the growth of the lava shield could have loaded and destabilized a pre-existing edifice. Catastrophic failure of a pyroclastic edifice and its marine-mud substrate is likely to have produced a chaotic/random series of dates in the resulting deposit. Instead, the inverted age sequence found could reflect a progressive 'top-down' incision of a nearby pyroclastic edifice with intercalated mud, built between ~650 to 4000 cal yrs BP. This hypothesis suggests that shield growth was preceded by intermittent pyroclastic activity, which lends support to the findings of Shane et al (2013) who report microscopic tephra layers from Rangitoto volcano preserved in lake sediments extending back to 1498 ± 140 cal yrs BP, suggesting an extended time-span for the volcano.

Regardless of the depositional history of the volcaniclastic deposits, the youngest age in the sequence (~650 cal yr BP) provides a maximum age for the shield-building stage represented by the overlying lava flows. A paleomagnetic investigation of the lava field (Robertson, 1986) revealed scatter in the demagnetized remnant directions, but much of the data is within wide error limits thereby preventing reliable interpretation of eruption duration. The only previous radiocarbon determinations associated with lava flows produced widely disparate ages of 214 ± 129 cal yrs BP for wood beneath a flow unit and 1161 ± 72 cal yrs BP for marine shells in mud baked by a (different) lava flow. These were dismissed by Nichol (1992) as representing young tree roots penetrating the lava flow, and relict shells pre-dating the eruption, respectively. However, the age of marine shells is in the range of ages obtained from the sub-surface sequence (Table 1).

If the tephra layers downwind of the volcano (Needham et al., 2011) reflect pyroclastic activity associated with summit scoria cones rather than the main shield-building stage, they then provide an upper age limit (~550-500 cal yrs BP) for shield development. This gives a maximum duration of about 100 years for shield growth. Continuity of eruption

during the shield-building stage is suggested by the lack of intercalated sediments and paleosols. However, the four composition groups erupted and the surface intercalation of lavas show that the shield was built in a series of closely spaced episodes, with one compositional change coinciding with a horizon of clay-filled fractures (at 95 m depth between Groups 1 and 2), which may indicate a pause of a few years to decades.

Magma evolution

Clustering of major element compositions according to stratigraphic position on variation diagrams demonstrates that the entire sub-surface sequence is not part of a single differentiation trend (Fig. 5,8).

Previous workers have highlighted the importance of batch partial melting of mantle sources to explain much of the compositional variation in Rangitoto (and other AVF basalts), based on trace element and radiogenic isotope data (see Huang et al., 1997; McGee et al., 2011; 2013). The more alkalic and incompatible element-enriched composition of the North Cone basalts is considered to reflect a lower degree of partial melting and a deeper, garnet-bearing source (asthenosphere), while sub-alkalic compositions, such as those of the Rangitoto lava field, are considered to involve the mixing of these partial melts with shallower spinel-bearing lithosphere (McGee et al., 2011). Thus, the magmatic system is viewed as a column involving the mixing of partial melts from a range of depths. Uniform Sr-Nd-Pb isotope ratios (albeit some diversity in North Cone magma) indicate a broadly common source for all Rangitoto basalts.

REE ratios can be used to assess the relative contribution of asthenospheric and lithospheric sources for the magmas. McGee et al. (2013) utilized a plot of $(Gd/Yb)_N$ (chondrite-normalized) as a proxy for garnet in the source, reflecting the compatibility of HREE in garnet, versus $(La/Yb)_N$ as a proxy for degree of partial melting, reflecting the high incompatibility of La. Rangitoto magmas and those of some other AVF volcanoes plot on linear mixing lines between model curves depicting partial melting of a garnet-bearing peridotite source (asthenosphere) and a spinel-bearing peridotite source (lithosphere).

We followed the same modelling to investigate the sub-surface basalt suite from the Rangitoto core. The suite plots between the two model melting curves and could be produced by mixing melts derived from 2-3% partial melting of garnet-peridotite and 1-2% partial melting of spinel-peridotite at approximately a 20:80 ratio, similar to that concluded by McGee et al. (2013) (Fig. 9A). The $(Gd/Yb)_N$ compositions show no discernable temporal trend with variation within error (Fig. 9B), suggesting the magmas were derived from the same mixture of melts throughout the eruption episode. However, $(La/Yb)_N$ compositions indicate the earliest magmas (Group 1) were produced by the lowest degree of melting (Fig. 9C). The succeeding Group 2 magmas (and Group 3, albeit less well defined) display a systematic trend of increasing degree of melting within each group. In general, the ratio of moderately incompatible to highly incompatible elements should increase as melting progresses, especially at low degrees of partial melting. This is evident in incompatible element ratios of Group 2 and 3 magmas (e.g., Zr/Nb and Nd/La, Fig. 6). These trends are not due to FC because compatible elements such as Mg, Ni, and Cr do not vary systematically with respect to stratigraphy within the groups. Similarly, mixing of melts of different proportions from a lithosphere and asthenosphere source, as modelled by McGee et al. (2013), is not favored as a mechanism because the $(Gd/Yb)_N$ proxy for such mixing is invariant (Fig. 9B).

Similar systematic trends in incompatible element concentrations within individual eruption sequences have been reported at other volcanoes, notably the Koloa volcanics, Kauai, and Big Pine Volcanic Field, California. Unlike Rangitoto volcano, there is some correlation to isotopic variation, reflecting separate mantle sources at these volcanoes

(Reiners and Nelson, 1998; Blondes et al., 2008). A magma plumbing system involving partial melting of a heterogeneous mantle (perhaps in the form of compositional veins of different solidi) and/or a mixture of melts from a range of depths has been proposed for causing such compositional zonation (e.g., Reiners and Nelson, 1998; Reiners 2002; Blondes et al., 2008). Melt-mantle interaction during channelized magma ascent through a homogeneous source region has also been modelled as a possible cause of incompatible element variation (Spiegelman and Kelemen, 2003). These authors suggest the that centers of channels contain enriched melts from depth, while the channel edges transport depleted melts extracted at shallower depths. Thus, sequentially tapping of a channel could produce compositional trends on short spatial and temporal scales. This could be significant for Rangitoto magmas because they lack isotopic variation indicating a common source.

Regardless of the mechanism, the Rangitoto Group 2 and 3 magmas represent pulses of melting presumably reflecting thermal perturbations. The shield-building stage represents a maximum period of about 100 years, thus placing an upper limit on the frequency and duration of such phenomena. It is not obvious why other magma batches lack temporal composition trends. It can only be speculated that the uniformity of fusion characteristics in the source and ascent rates could provide additional insight.

History of the volcano

The construction of Rangitoto volcano can be divided into three major magmatic and eruptive phases. Phase 1 includes the oldest lava flow (~6,000 cal yr BP) and overlying volcaniclastic deposits. These units are compositionally indistinguishable from the lowermost shield-building lava flows (Group 1) that post-date ~650 cal yr BP. Collectively this represents a phase of prolonged and/or periodic tapping a common magma. Compared to the rest of the volcano history, magmatic output was low during this phase until the end when shield-building lava flows commenced.

Phase 2 comprises the main lava shield-building stage when magma production significantly increased for a short period at ~650-550 cal yr BP. Cycles of increasing degree of melting at the mantle source occurred (Group 2 and 3 magma), presumably representing thermal perturbations. This represents a significant change in the magmatic and eruptive behavior. The final shield-building magma (Group 4 lava flows) is more differentiated (lower Mg#) consistent with a higher degree of FC. However, trace element compositions exclude earlier erupted magmas (Groups 1-3) as direct parents. This points to tapping of a heterogeneous mantle source, in addition to a change in magma dynamics promoting FC.

Phase 3 represents a change to pyroclastic volcanism and the construction of summit scoria cones at ~550-500 cal yrs BP. At this time, the magmatic system was compositionally more diverse, but volumetrically less productive. While Central and South Cones are compositionally similar to the shield-building lava flows, they also erupted lower-Mg# magma. In contrast, North Cone is distinctly alkalic and REE ratios suggest the dominance of a deep garnet-bearing source and small degrees of partial melting (Fig. 9A).

The eruption of multiple magma batches both sequentially and simultaneously has been reported at other small basaltic volcanoes, in particular in the Newer Volcanics Province (van Otterloo et al., 2014; Boyce et al., 2015). Changes in magmatic compositions at these and other small volcanoes (e.g., Strong and Wolff, 2003) often accompany changes in eruption style, such as effusive versus explosive. However, no overriding temporal trends are evident. Of the few AVF volcanoes for which temporally-controlled data is available, there is a lack of common compositional evolution (e.g., Smith et al., 2008; McGee et al., 2012; this study). This points to the localized influence of mantle heterogeneity and conduit systems.

In the traditional concept of ‘monogenetic’ volcanism, magmas ascend from mantle sources without crustal storage episodes, and thus, a thermally and mechanically favorable

conduit is not maintained following eruption unless there is a high magma supply rate (e.g., Walker, 1993). Significant upper crustal residence is seemingly unlikely for Rangitoto magmas (McGee et al., 2011). Thus, the prolonged life of the volcano (~6 ka) demonstrates reactivation of deep conduit systems occurred despite the low magma supply (a total of ~0.7 km^3 for Rangitoto). Crustal structure beneath the volcano is unknown. Thus, the role of factors that contributed to magma pathways, such as contemporaneous intrusion prolonging thermally favorable conditions, is unknown.

Implications for hazards

From a future hazards prospective, the new insights to Rangitoto volcano raise the possibility that it could erupt again via the same magmatic source. By inference, other AVF volcanoes with large lava fields (e.g., One Tree Hill, Mt. Eden) (Kereszturi et al. 2013) could have displayed this type of eruptive behavior in the past, but little is known about their sub-surface deposits. Future eruptions in AVF could last for decades and involve large-volume outpourings of sub-alkalic basalt. It is uncertain how long a mantle magma source for small intra-plate basalt volcanoes may be productive and generate eruptions, but the Rangitoto chronology indicates a minimum duration of ~6 ka. Elsewhere, eruption hiatuses on the 10^5 years-scale have been reported at some volcanoes (e.g., Brenna et al., 2015), but the co-location of activity could be coincidental. The prolonged and varied pattern of behavior of Rangitoto volcano is consistent with other recently investigated volcanoes in monogenetic basaltic fields (e.g., Newer Volcanics Province, Boyce, 2013), and may require a change in emphasis in hazard scenario modelling.

ACKNOWLEDGEMENTS

Drilling and geochemical analyses were funded by Earthquake Commission Biennial Grant Programme 14/676 and Post-Graduate Research Programme grant 14/684. Additional funds for radiocarbon dating were provided by Auckland City Council. We thank Pro-Drill Ltd and Alton Drilling Ltd for their expertise. Roland Maas assisted in obtaining radiogenic isotope data. Paul Augustinus assisted with obtaining radiocarbon ages. Some of the radiocarbon ages were funded by Auckland City Council.

REFERENCES CITED

Bebbington, M.S., and Cronin, S.J. 2011, Spatio-temporal hazard estimation in the Auckland Volcanic Field, New Zealand, with a new event-order model. Bulletin of Volcanology v. 73, p. 55–72, doi:10.1007/s00445-010-0403-6.

Blondes, M.S., Reiners, P.W., Ducea, M.N., Singer, B.S., and Chesley, J., 2008, Temporal-compositional trends over short and long time-scales in basalts of the Big Pine Volcanic Field, California. Earth and Planetary Science Letters, v. 269, p.140-154.

Boyce, J., 2013, The Newer Volcanics Province of southeastern Australia: a new classification scheme and distribution map for eruption centres. Australian Journal of Earth Sciences: An International Geoscience Journal of the Geological Society of Australia, v. 60, p. 449-462.

Boyce, J.A., Nichols, I.A., Keays, R.R., and Hayman, P.C. 2015, Variation in parental magmas of Mt Rouse, a complex polymagmatic monogenetic volcano in the basaltic intraplate Newer Volcanics Province, southeast Australia. Contributions to Mineralogy and Petrology, v. 169, 11. DOI 10.1007/s00410-015-1106-y.

Brenna, M., Cronin, S., Smith, I., Sohn, Y., and Nemeth, K., 2010, Mechanisms driving polymagmatic activity at a monogenetic volcano, Udo, Jeju Island, South Korea. Contributions to Mineralogy and Petrology, v. 160, p. 931-950.

Brenna, M., Nemeth, K., Cronin, S.J., Sohn, Y.K., Smith, I.E., and Wijbrans, J., 2015, Co-located monogenetic eruptions similar to 200 kyr apart driven by tapping vertically separated mantle source regions, Chagwido, Jeju Island, Republic of Korea. Bulletin of Volcanology v. 77, 43. DOI 10.1007/s00445-015-0928-9.

Eggins, S.M., Kinsley, L.P.J., and Shelley, J.M.G., 1998, Deposition and element fractionation processes during atmospheric pressure laser sampling for analysis by ICP-MS. Applied Surface Science, v. 127- 129, p. 278-286.

Ersoy, Y. and Helvaci, C., 2010, FC-AFC-FCA and mixing modeller: A Microsoft Excel spreadsheet program for modeling geochemical differentiation of magma from crystal fractionation, crustal assimilation and mixing: Computers and Geosciences, v. 36, p. 383 – 390.

Harvey, P.K., Taylor, D.M., Hendry, R.D., and Bancroft, F., 1973, X-ray spectrometry, *in*, An Accurate Fusion Method for the Analyses of Rocks and Chemically Related Materials by X-Ray Fluorescence Spectrometry, pp. 33–44, Heyden and Son, London.

Hogg, A.G., Hua, Q., Blackwell, P.G., et. al., 2013, SHCal13 Southern Hemisphere Calibration, 0–50,000 years cal BP. Radiocarbon, v. 55, p. 1889–1903.

Horspool, N.A., Savage, M.K., and Bannister, S., 2006, Implications for intraplate volcanism and back-arc deformation in northwestern New Zealand, from joint inversion of receiver functions and surface waves. Geophysical Journal International, v. 166, p. 1466–1483.

Houghton, B.F., Bonadonna, C., Gregg, C.E., et al., 2006, Proximal tephra hazards: Recent eruption studies applied to volcanic risk in the Auckland volcanic field, New Zealand. Journal of Volcanology and Geothermal Research, v. 155, p. 138-149.

Huang, Y. M., Hawkesworth, C., van Calsteren, P., Smith, I., and Black, P., 1997, Melt generation models for the Auckland volcanic field, New Zealand: Constraints from U-Th isotopes. Earth and Planetary Science Letters, v. 149, p. 67-84.

Irvine,T. N., and Baragar, W.R.A., 1971, A guide to the chemical classification of the common volcanic rocks. Canadian Journal of Earth Sciences, v. 8, p. 523-548.

Jordan, S.C., Jowitt, S.M., Cas, R.A.F., 2015, Origin of temporal - compositional variations during the eruption of Lake Purrumbete Maar, Newer Volcanics Province, southeastern Australia. Bulletin of Volcanology, v. 77:883. DOI 10.1007/s00445-014-0883-x.

Jordan, S.C., Cas, R.A.F., Hayman, P.C., 2013, The origin of a large (>3km) maar volcano by coalescence of multiple shallow craters: Lake Purrumbete maar, southeastern Australia. Journal of Volcanology and Geothermal Research, v. 254, p. 5–22.

Kereszturi, G., Cappello, A., Ganci, G., Procter, J., Németh, K., Del Negro, C., and Cronin, S.J., 2014, Numerical simulation of basaltic lava flows in the Auckland Volcanic Field, New Zealand – implication for volcanic hazard assessment. Bulletin of Volcanology, v. 76, p. 879-896.

Le Maitre, R.W., 2002, Igneous Rocks: A Classification and Glossary of Terms. Cambridge University Press, 236 p.

Lindsay, J.M., Leonard, G.S, Smid, E.R., and Hayward, B.W., 2011, Age of the Auckland Volcanic Field: a review of existing data. New Zealand Journal of Geology and Geophysics, v. 54, p. 379-401.

Maas, R., Kamenetsky, M.B., Sobolev, A.V., Kamenetsky, V.S., and Sobolev, N.V., 2005, Sr, Nd, and Pb isotope evidence for a mantle origin of alkali chlorides and carbonates in the Udachnaya kimberlite, Siberia. Geology, v. 33, p. 549 –522.

McGee, L.E., Beier, C., Smith, I.E.M., et al., 2011, Dynamics of melting beneath a small-scale basaltic system: a U-Th-Ra study from Rangitoto volcano, Auckland volcanic field, New Zealand. Contributions to Mineralogy and Petrology, v. 162, p. 547-563. DOI: 10.1007/s00410-011-0611-x.

McGee, L.E., Millet, M.-A., Smith, I.E.M., Nemeth, K., and Lindsay, J.M., 2012, The inception and progression of melting in a monogenetic eruption: Motukorea Volcano, the Auckland Volcanic Field, New Zealand. Lithos, v. 155, p. 360-374.

McGee, L.E., Smith, I.E.M., Millet, M.-A., Handley, H.K., and Lindsay, J.M., 2013, Asthenospheric control of melting processes in a monogenetic basaltic system: a case study of the Auckland Volcanic Field, New Zealand. Journal of Petrology, v. 54, p. 2125-2153.

Milligan, J.A., 1977, A geophysical study of Rangitoto Volcano. Unpublished MSc Thesis, University of Auckland.

Needham, A.J,, Lindsay, J.M., Smith, I.E.M., Augustinus, P., and Shane, P.A., 2011, Sequential eruption of alkaline and sub-alkaline magmas from a small monogenetic volcano in the Auckland Volcanic Field, New Zealand. Journal of Volcanology and Geothermal Research, v. 201, p. 126-142. doi:10.1016/j.jvolgeores.2010.07.017.

Nichol, R., 1992, The eruption history of Rangitoto: reappraisal of a small New Zealand myth. Journal of the Royal Society of New Zealand, v. 22, 159-180.

Reimer, P. J., Bard, E., Bayliss, A., et al., 2013, INTCAL13 and MARINE13 radiocarbon age calibration curves 0–50,000 years cal BP. Radiocarbon, v. 55, p. 1869–1887.

Reiners, P.W., 2002, Temporal-compositional trends in intraplate basalt eruptions: implications for mantle heterogeneity and melting processes. Geochemistry, Geophysics, Geosystems, v. 3, doi: 10.1029/ 2001GC000250.

Reiners, P., and Nelson, B, 1998, Temporal-compositional-isotopic trends in rejuvenated-stage magmas of Kauai, Hawaii, and implications for mantle melting processes. Geochimica et Cosmochimica Acta, v. 62, p. 2347-2368.

Robertson, D.J., 1986, A paleomagnetic study of Rangitoto Island, Auckland, New Zealand. New Zealand Journal of Geology and Geophysics, v. 29, p. 405-411.

Shane, P., Gehrels, M., Zawalna-Geer, A., Augustinus, P., Lindsay, J., and Chaillou, I., 2013, Longevity of a small shield volcano revealed by crypto-tephra studies (Rangitoto volcano, New Zealand): change in eruptive behavior of a basaltic field. Journal of Volcanology and Geothermal Research, v. 257, p. 174-183. 10.1016/j.jvolgeores.2013.03.026.

Spiegelman, M., and Kelemen, P.B., 2003, Extreme chemical variability as a consequence of channelized melt transport. Geochemistry Geophysics Geosystems, v.4, 1055, doi:10.1029/2002GC000336.

Smith, I.E.M., Blake, S., Wilson, C.J.N., et al., 2008, Deep-seated fractionation during the rise of a small-volume basalt magma batch: Crater Hill, Auckland, New Zealand. Contributions to Mineralogy and Petrology, v. 155, p. 511-527, doi: 10.1007/s00410-007-0255-z.

Stracke, A., Bizimis, M., and Salters, V.J.M., 2003, Recycling oceanic crust: quantitative constraints. Geochemistry, Geophysics, Geosystems, v. 4, doi:10.1029/2001GC000223.

Stracke, A., Hofmann, A.W., and Hart, S.R., 2005, FOZO, HIMU and the rest of the mantle zoo. Geochemistry, Geophysics, Geosystems, v. 6, doi:10.1029/2004GC000824.

Strong, M., and Wolff, J., 2003, Compositional variations within scoria cones. Geology, v. 31, p. 143–146.

Sun, S.S., and McDonough, W.F., 1989, Chemical and isotopic systematics of oceanic basalts: Implications for mantle composition and processes, *in*, Saunders, A.D., and Norry, M.J., eds, Magmatism in the Ocean Basins, Geological Society Special Publication, v. 42, p. 313–345.

van Otterloo, J., Raveggi, M., Cas, R.A.F, Maas, et al., 2014, Polymagmatic activity at the monogenetic Mt Gambier Volcanic Complex in the Newer Volcanics Province, SE Australia: new insights into the occurrence of intraplate volcanic activity in Australia. Journal of Petrology, v. 55, p. 1317-1351.

Walker, G.P.L., 1993, Basaltic-volcano systems, *in*, Prichard, H.M., Alabaster, T., Harris, N.B.W., Neary, C.R., eds., Magmatic processes and plate tectonics. Geological Society, London, pp 3–38.

Wood, C., 1980, Morphometric evolution of cinder cones. Journal of Volcanology and Geothermal Research, v. 7, p. 387-413.

Woodhead, J.D., 2002, A simple method for obtaining highly accurate Pb isotope data by MC-ICP-MS, Journal of Analytical Atomic Spectrometry, v. 17, p. 1-6.

Figure captions

Figure 1. (a) Map of the Auckland Volcanic Field, New Zealand, and (B) Rangitoto volcano showing the location of the drill site, and outcrops of basalt classified into groups reflecting the geochemistry of sub-surface lava flows (see text). (C) Simplified cross sections of Rangitoto volcano from Needham et al. (2011) (top) and based on this study (bottom).

Figure 2. Lithological log of the Rangitoto drill core showing petrological sample locations.

Figure 3. Lithological log of the basal sequence of the Rangitoto drill core showing the location and ages of samples collected for ^{14}C dating.

Figure 4 Composition of Rangitoto sub-surface basalts from the drill core. (A) Classification plot of the basalt field defined by La Maitre (2002). Alkalic/sub-alkalic boundary as defined by Irvine and Baragar (1971). (B) Incompatible multi-element diagram, normalized to primitive mantle following Sun & McDonough (1989). (C) Radiogenic isotope compositions. North Cone basalt shown for comparison. Compositional fields for Pacific MORB, HIMU and FOZO from Stracke et al. (2003; 2005).

Figure 5. Major and trace element chemistry of Rangitoto sub-surface basalts plotted against Mg#. Elements selected to represent the diversity of compositions displayed in the rock suite.

Figure 6 Geochemistry and isotopic composition of Rangitoto sub-surface basalts plotted against stratigraphic depth in the drill core. Elements were selected to represent the diversity of compositions displayed in the rock suite.

Figure 7 Compositional fields of Rangitoto sub-surface basalts compared to analyses of basalts from outcrops from Needham et al. (2011). Refer to Fig. 1B for outcrop distribution.

Figure 8. Rayleigh fractional crystallization model curves based on a mafic parent (sample 44 of Group 3, Mg# 64), and extracting clinopyroxene and olivine in a 33:67 ratio as indicated by mass balance calculations (Table 4) and modal mineralogy of the rocks. Models generated by software and using partition coefficients in Ersoy and Helvaci (2010).

Figure 9. (a) REE ratios for the Rangitoto basalt sub-surface sequence and North Cone showing possible melting and mixing processes following the models of McGee et al. (2012; 2013). Melting curves denotes melting of a garnet peridotite source (asthenosphere) and a spinel-bearing peridotitic source (lithosphere). Numbers on model curves denote degrees of partial melting. Straight lines connecting the curves represent mixing lines. See McGee et al. (2012; 2013) for starting compositions and partition coefficients. (B) Proxy for mixing of melts (Gd/Yb) plotted against stratigraphic order of sub-surface lava samples. (C) Proxy for degree of partial melting at source (La/Yb) plotted against stratigraphic order of sub-surface lava samples.

TABLE 1. ACCELERATOR MASS SPECTROMETRY AGES

Sample ID	Core depth (m)	Material	Age ID NZA	Radiocarbon age (yrs BP)	error (yrs)	□13C (‰) ±0.2	Calibrated age (yrs BP)	error (yrs)
R1-009	128	shell	57098	3875	23	-1.59	3840	50
R1-009b	128.1	gastropod	58368	3962	23	1.7	3960	50
R1-132.18	132.18	bivalve	58944	3151	27	1.6	2930	50
R1-133.08	133.08	seed	59043	1708	20	-24.6	1570	30
R1-063	133.11	shell	57100	2010	20	-0.22	1570	40
R1-135.32	135.32	forams	58943	1092	26	0	650	30
R1-064	135.39	shell	57101	1429	20	1.18	970	30
R1-068	136.5	shell	57103	5591	25	2.37	5980	50
R1-068b	136.5	wood	58337	5190	19	-27	5900	60
R1-067b	137.26	gastropod	58367	6401	26	0.7	6880	50
R1-137.32	137.32	gastropod	58942	6478	32	1	6980	60
R1-067	137.84	gastropod	57102	6411	27	0.72	6890	50
R1-035	139.38	shell	57099	6927	28	2.56	7438	30

Shell = Mollusc shell fragment
Note the cal ages are ± 2 sigma

TABLE 2. Sr-Nd-Pb ISOTOPE COMPOSITION OF BASALTS IN THE CORE AND NORTH CONE (NC)

Depth (m)	Sample	$^{87}Sr/^{86}Sr$ ±0.00004	$^{143}Nd/^{144}Nd$ ±0.00002	$^{206}Pb/^{204}Pb$ ±0.05%	$^{207}Pb/^{204}Pb$ ±0.05%	$^{208}Pb/^{204}Pb$ ±0.08%
8.92	57	0.703021	0.512944	19.049	15.595	38.754
21.88	54	0.703061	0.512939	19.055	15.600	38.767
28.22	63	0.703047	0.512947	19.037	15.593	38.737
				19.040	15.597	38.749
42.87	46	0.703069	0.512973	19.045	15.595	38.747
55.02	43	0.703029	0.512968	19.049	15.589	38.729
66.49	41	0.703017	0.512959	19.046	15.596	38.749
69.44	40	0.703053	0.512963	19.051	15.600	38.762
80.45	39	0.703045	0.512972	19.067	15.603	38.779
90.38	62	0.702996	0.512977	19.059	15.589	38.736
		0.702969				
97.07	37	0.702985	0.512983	19.064	15.589	38.739
120.24	60	0.702990	0.512962	19.058	15.589	38.735
NC	59319	0.702857	0.512998	19.174	15.589	38.813
		0.702788				

See text for analytical details and uncertainty estimates

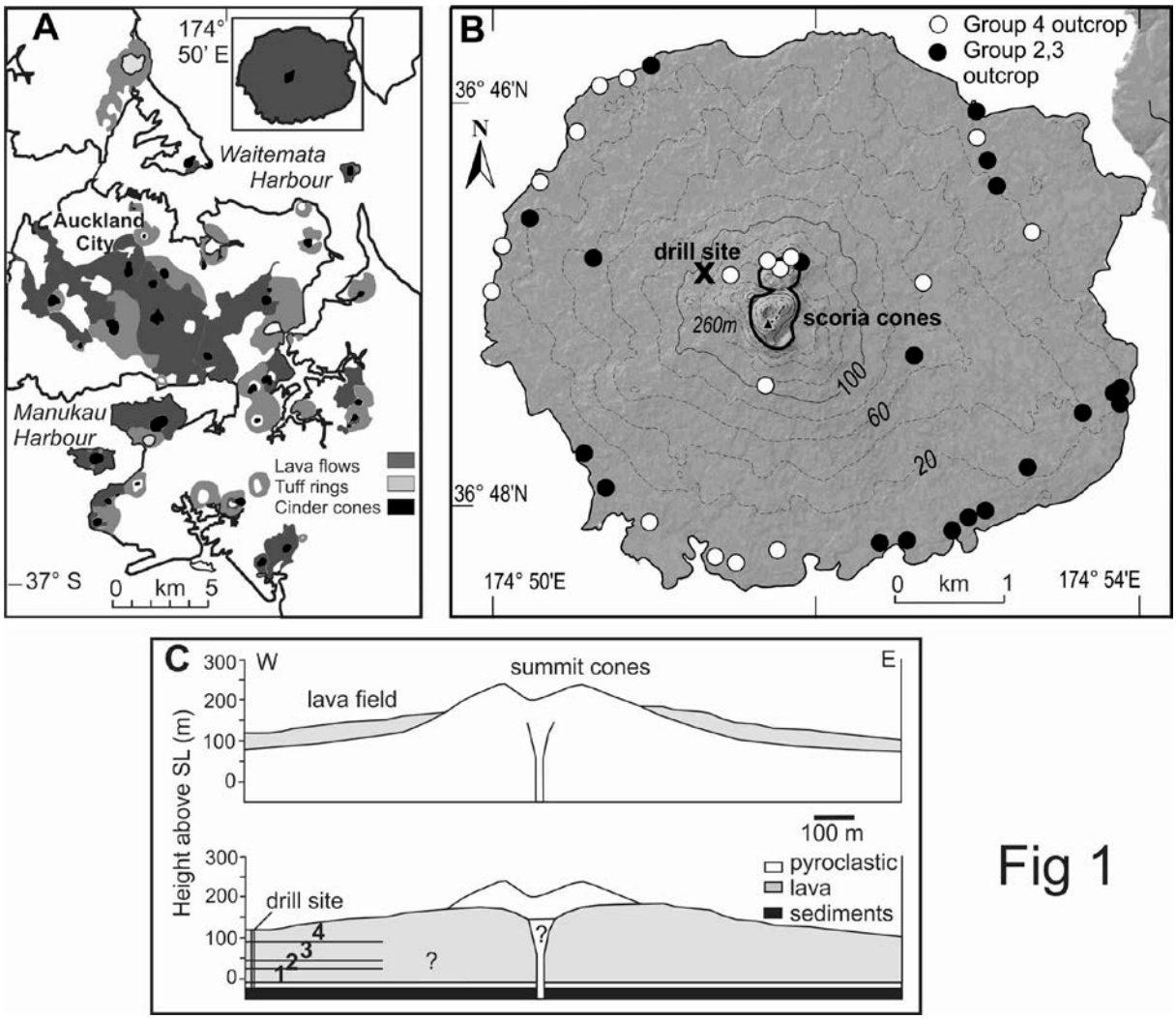
A
174° 50' E
Waitemata Harbour
Auckland City
Manukau Harbour
Lava flows
Tuff rings
Cinder cones
37° S
0 km 5
B
Group 4 outcrop
Group 2,3 outcrop
36° 46'N
N
drill site
260m
scoria cones
100
60
20
36° 48'N
174° 50'E
0 km 1
174° 54'E
C
W
E
summit cones
lava field
Height above SL (m)
300
200
100
0
100 m
pyroclastic
lava
sediments
drill site
1
2
3
4
?
?

Fig 1

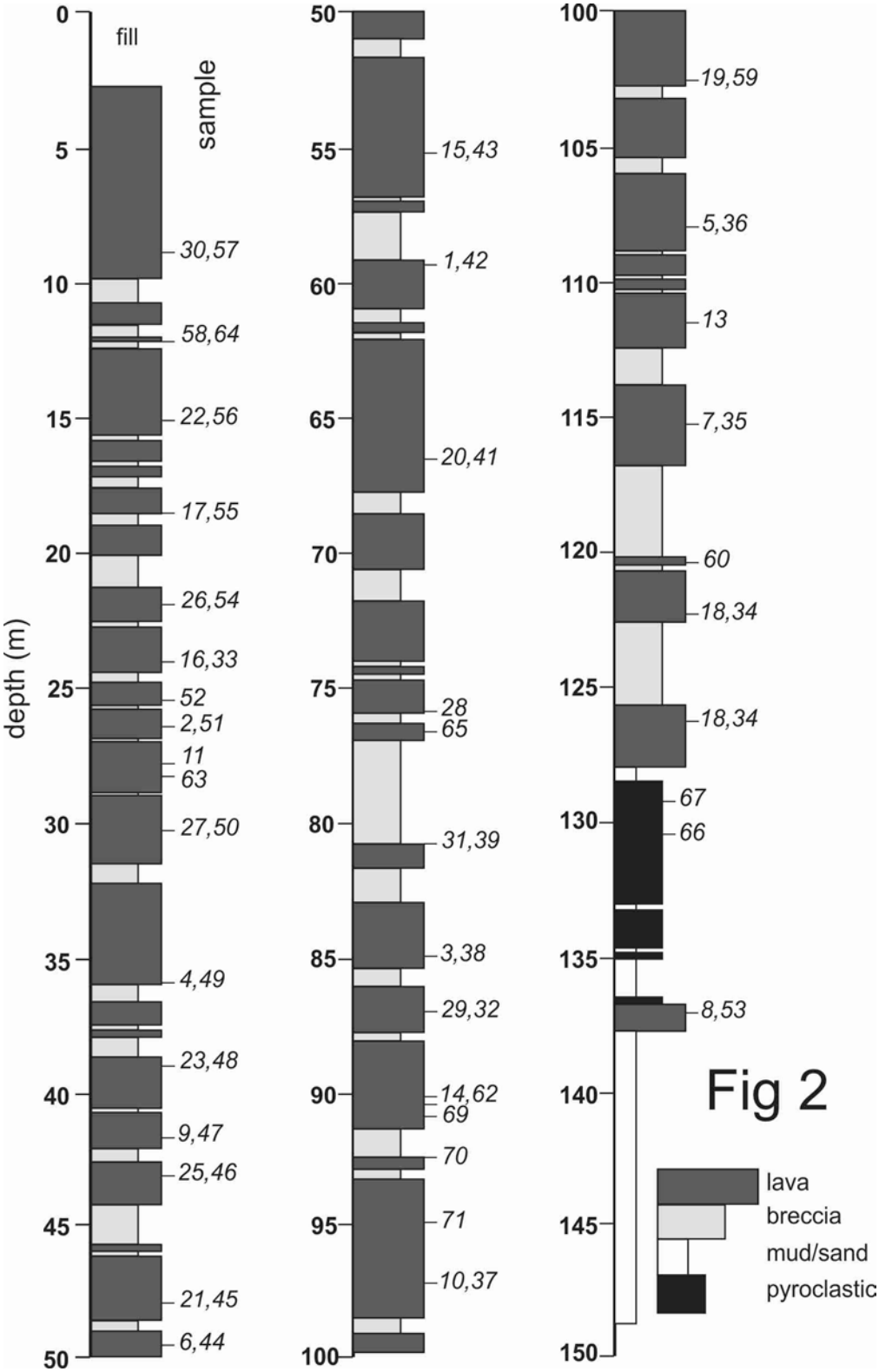
depth (m)
fill
sample
0
5
10
15
20
25
30
35
40
45
50
30,57
58,64
22,56
17,55
26,54
16,33
52
2,51
11
63
27,50
4,49
23,48
9,47
25,46
21,45
6,44
50
55
60
65
70
75
80
85
90
95
100
15,43
1,42
20,41
28
65
31,39
3,38
29,32
14,62
69
70
71
10,37
100
105
110
115
120
125
130
135
140
145
150
19,59
5,36
13
7,35
60
18,34
18,34
67
66
8,53
lava
breccia
mud/sand
pyroclastic

Fig 2

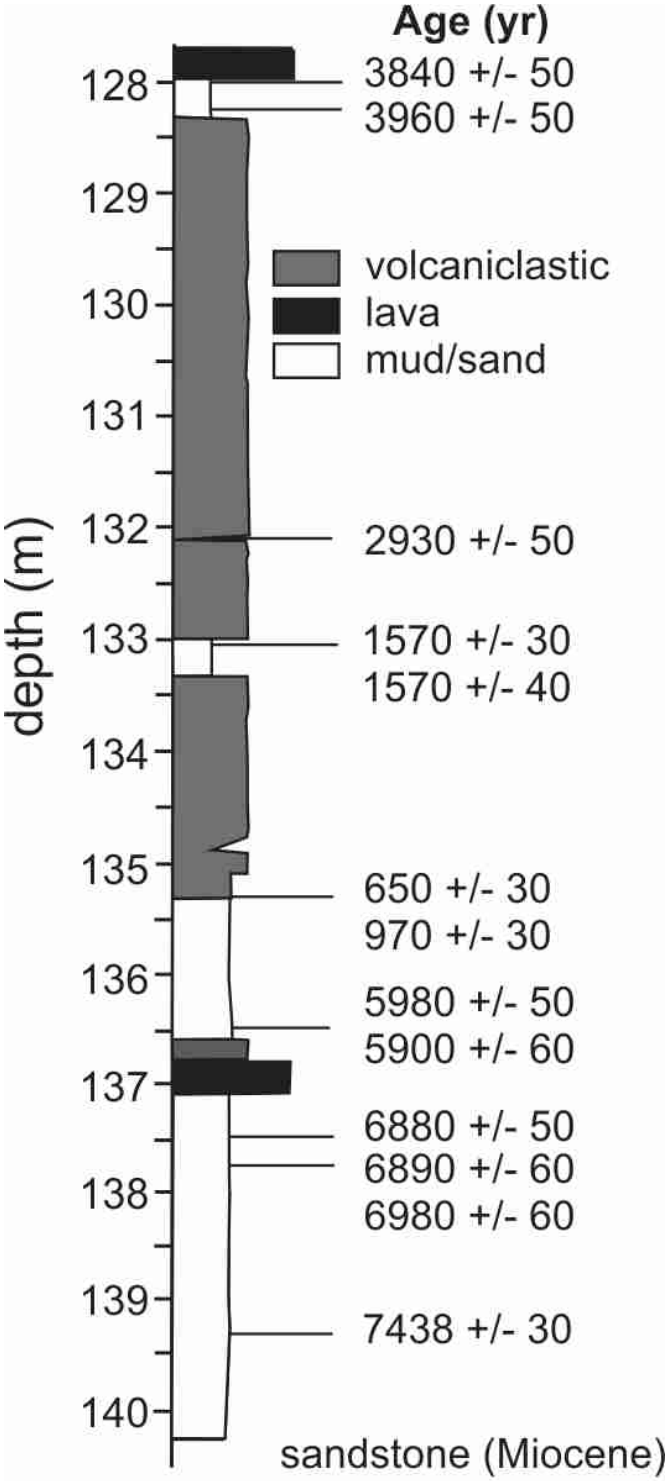
Age (yr)
3840 +/- 50
3960 +/- 50
volcaniclastic
lava
mud/sand
2930 +/- 50
1570 +/- 30
1570 +/- 40
650 +/- 30
970 +/- 30
5980 +/- 50
5900 +/- 60
6880 +/- 50
6890 +/- 60
6980 +/- 60
7438 +/- 30
depth (m)
128
129
130
131
132
133
134
135
136
137
138
139
140
sandstone (Miocene)

Fig 3

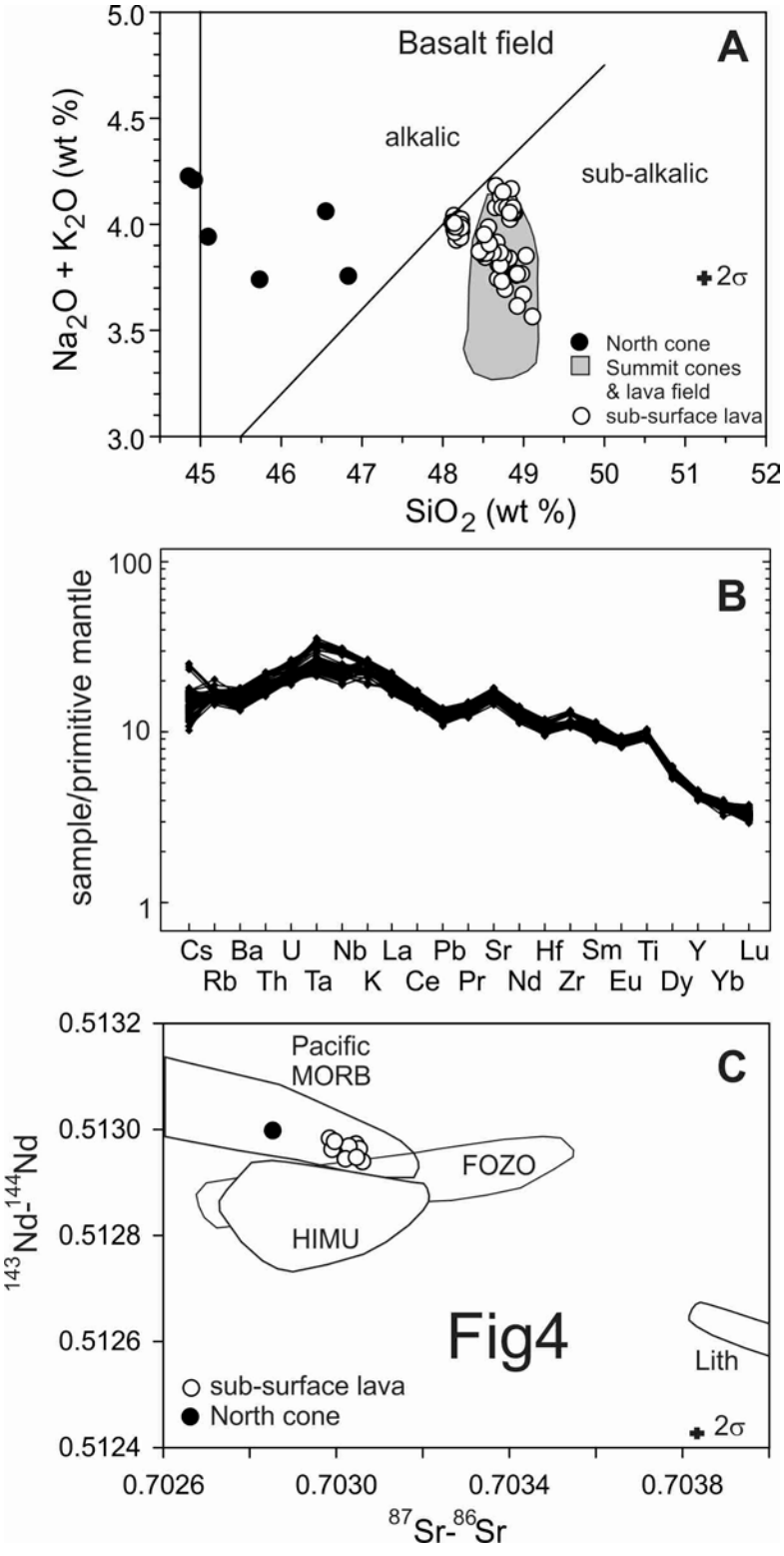
A
Basalt field
alkalic
sub-alkalic
2σ
North cone
Summit cones
& lava field
sub-surface lava
Na2O + K2O (wt %)
SiO2 (wt %)
5.0
4.5
4.0
3.5
3.0
45
46
47
48
49
50
51
52
B
sample/primitive mantle
100
10
1
Cs Ba U Nb La Pb Sr Hf Sm Ti Y Lu
Rb Th Ta K Ce Pr Nd Zr Eu Dy Yb
C
Pacific
MORB
FOZO
HIMU
Lith
2σ
sub-surface lava
North cone
143Nd-144Nd
87Sr-86Sr
0.5132
0.5130
0.5128
0.5126
0.5124
0.7026
0.7030
0.7034
0.7038
Fig4

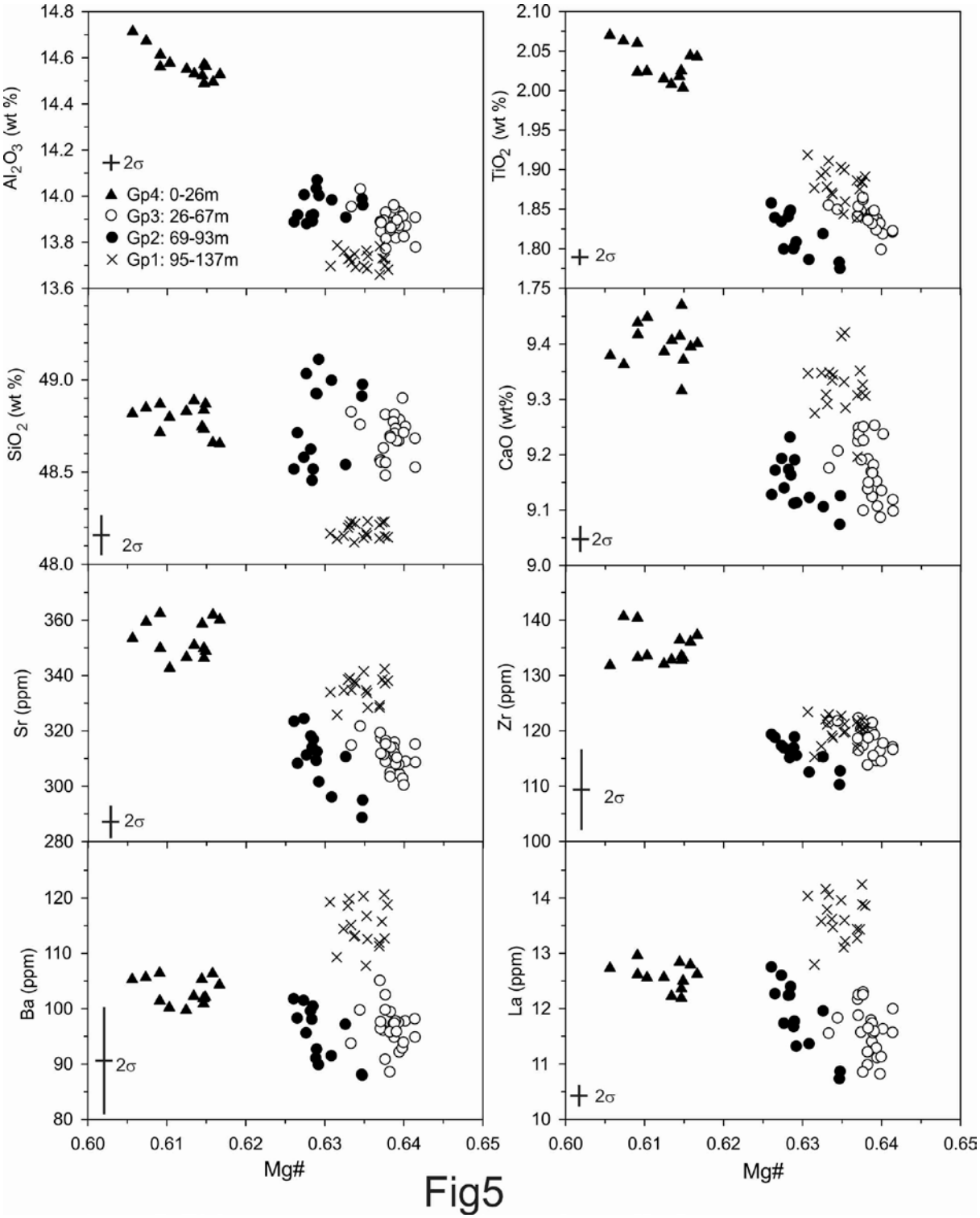
Al2O3 (wt %)
TiO2 (wt %)
SiO2 (wt %)
CaO (wt%)
Sr (ppm)
Zr (ppm)
Ba (ppm)
La (ppm)
Mg#
Mg#
2σ
Gp4: 0-26m
Gp3: 26-67m
Gp2: 69-93m
Gp1: 95-137m

Fig5

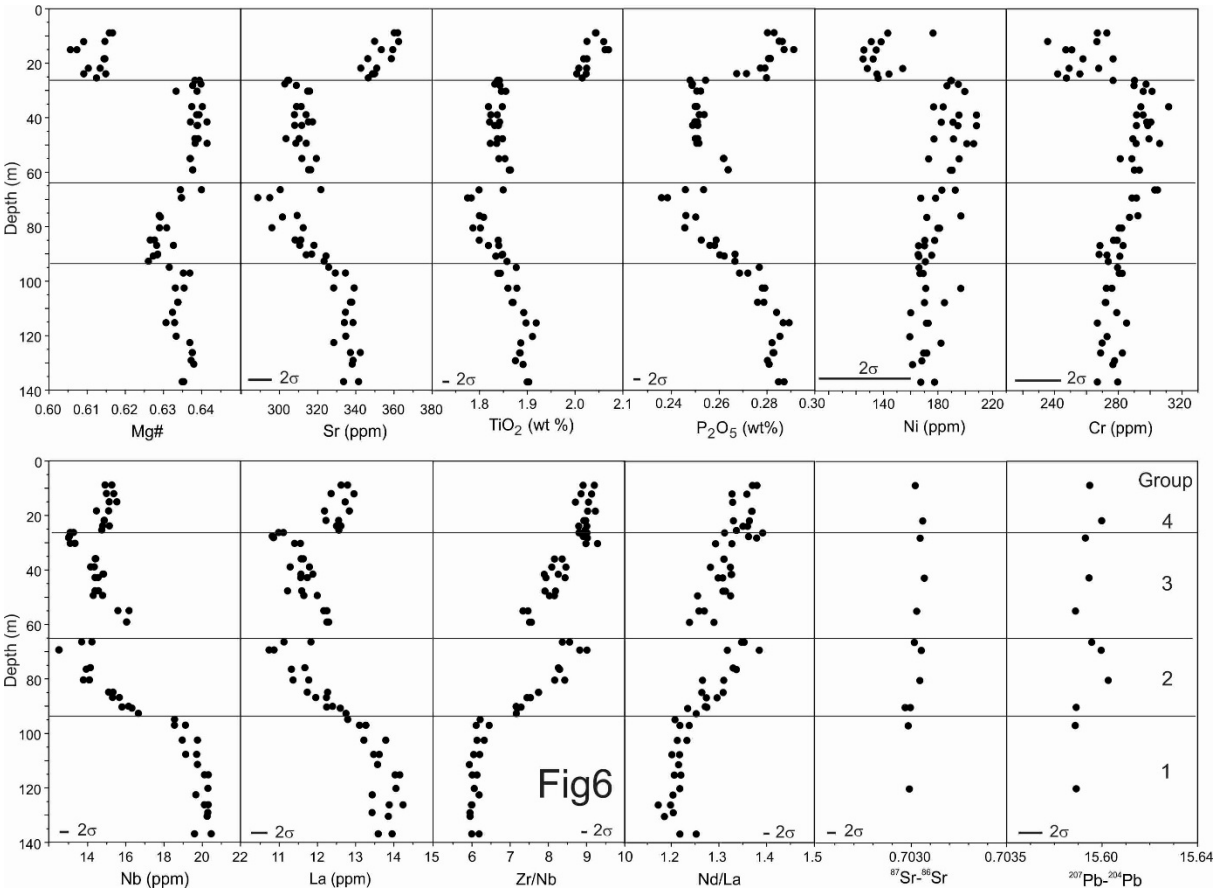
Depth (m)
Mg#
Sr (ppm)
TiO2 (wt %)
P2O5 (wt%)
Ni (ppm)
Cr (ppm)
Nb (ppm)
La (ppm)
Zr/Nb
Nd/La
87Sr-86Sr
207Pb-204Pb
Group
4
3
2
1
2σ
Fig6

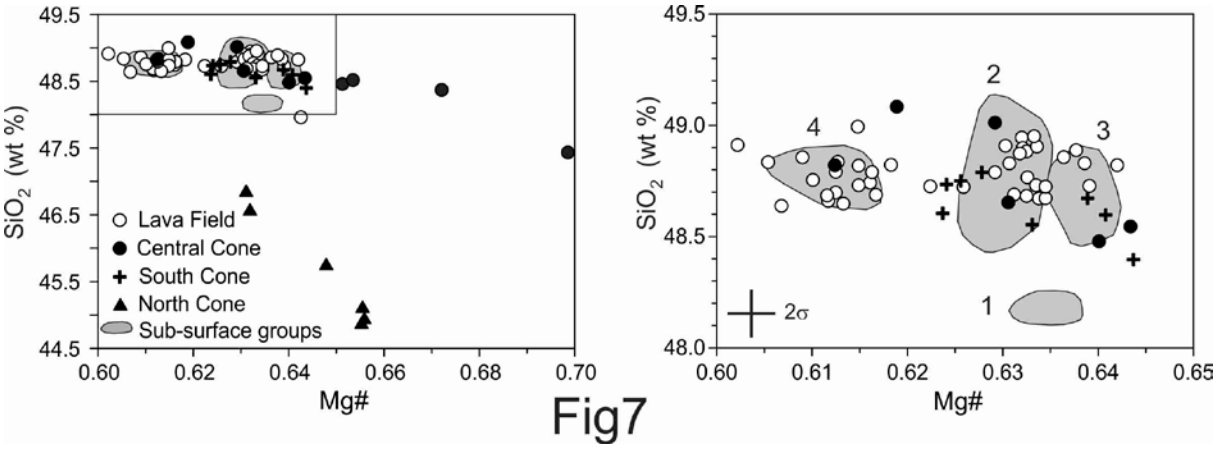
SiO2 (wt %)
Mg#
Lava Field
Central Cone
South Cone
North Cone
Sub-surface groups
2σ
1
2
3
4
Fig7

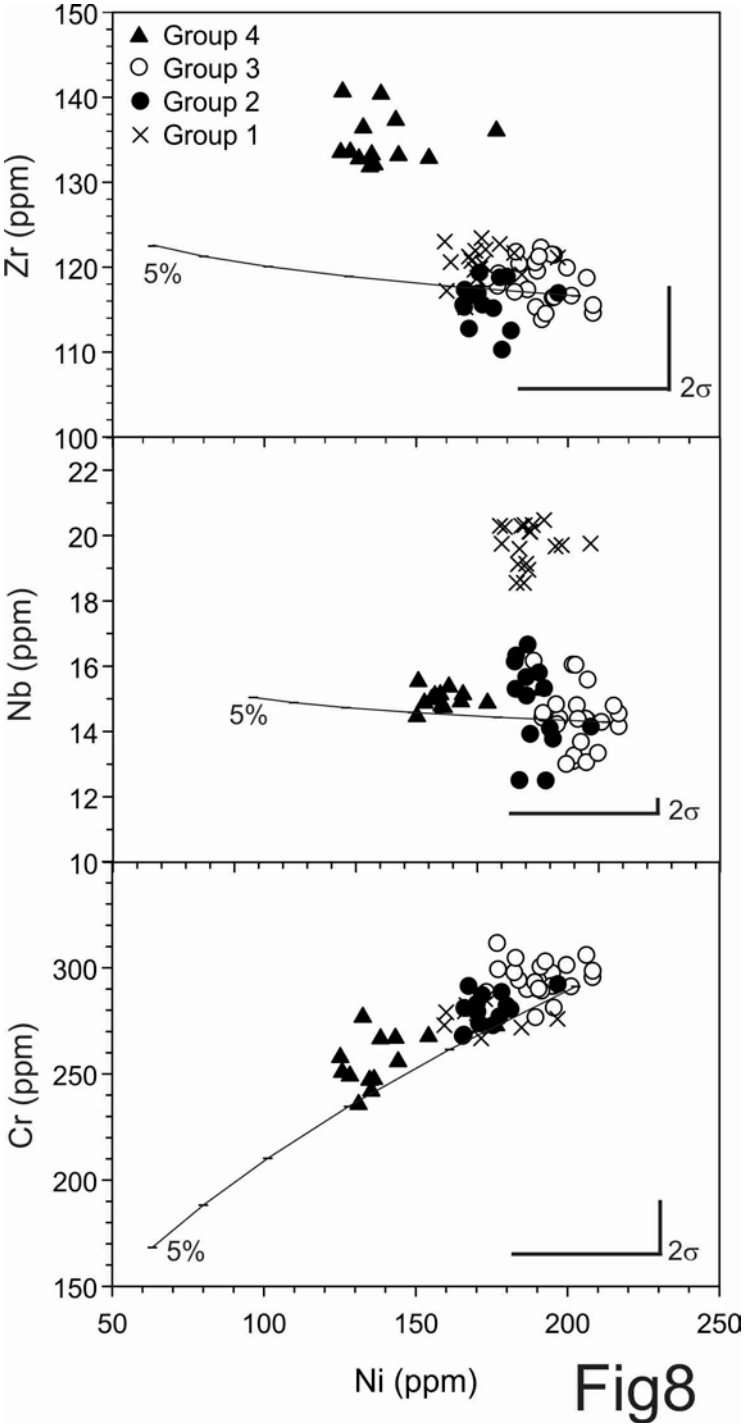

Fig8

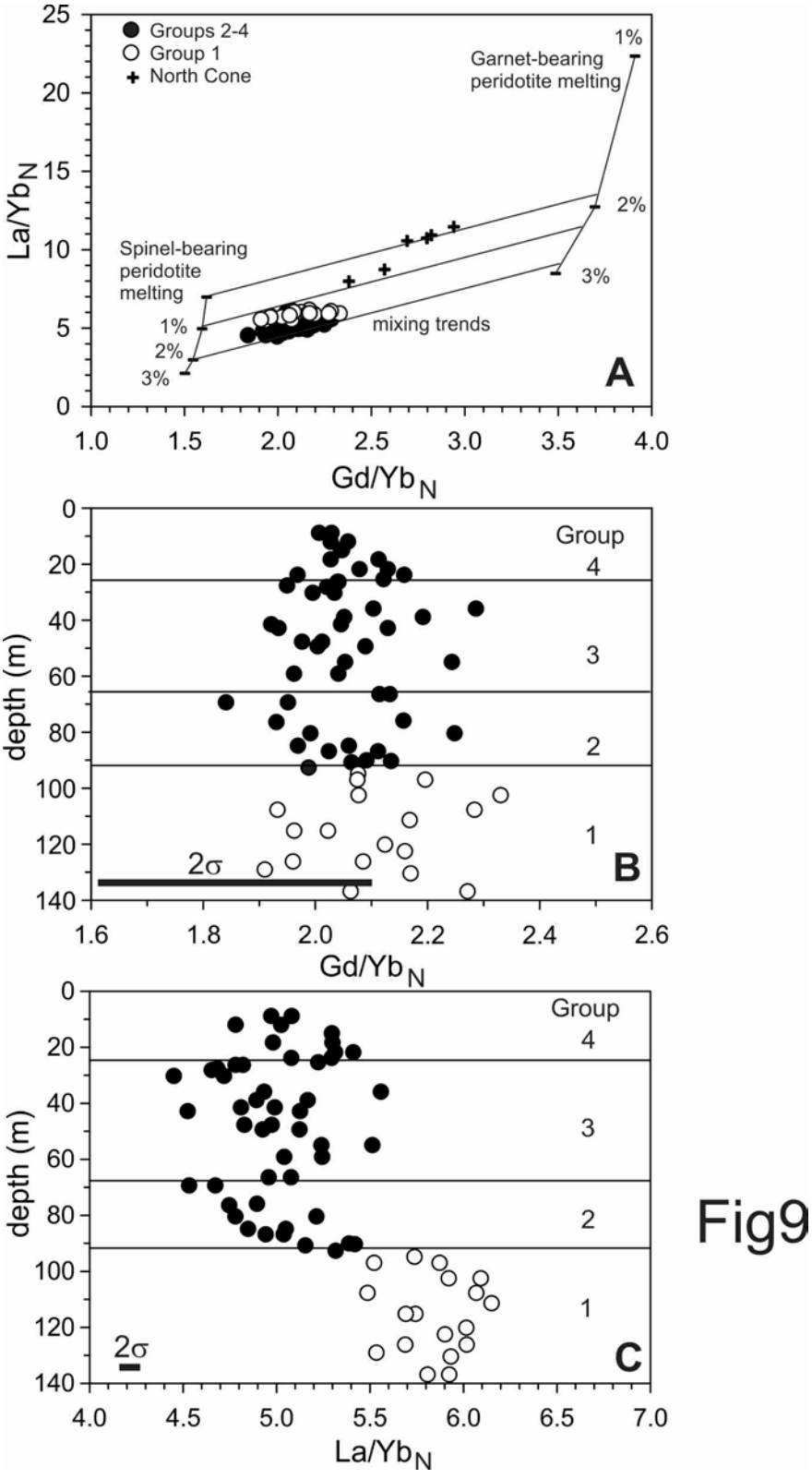
Groups 2-4
Group 1
North Cone
Garnet-bearing peridotite melting
1%
2%
3%
Spinel-bearing peridotite melting
1%
2%
3%
mixing trends
A
La/Yb N
Gd/Yb N
Group
4
3
2
1
depth (m)
2σ
B
Gd/Yb N
Group
4
3
2
1
depth (m)
2σ
C
La/Yb N

Fig9